Received: 9 October 2021 | Revised: 5 April 2022 | Accepted: 10 April 2022

DOI: 10.1002/eqe.3656

RESEARCH ARTICLE

WILEY

Experimental performance of a multi-storey braced frame structure with non-structural industrial components subjected to synthetic ground motions

Chiara Nardin[1] | **Oreste S. Bursi**[1] | **Fabrizio Paolacci**[2] | **Alberto Pavese**[3] | **Gianluca Quinci**[2]

[1]Department of Civil, Environmental and Mechanical Engineering, University of Trento, Trento, Italy

[2]Department of Engineering, Roma Tre University, Rome, Italy

[3]EUCENTRE Foundation, Pavia, Italy

Correspondence
Oreste S. Bursi, Department of Civil, Environmental and Mechanical Engineering, University of Trento, Via Mesiano 77, 38123 Trento, Italy.
Email: oreste.bursi@unitn.it

Funding information
HORIZON 2020 Framework Programme; Italian Ministry of Education, University and Research

Abstract

The seismic risk assessment of industrial facilities mainly relies on historical data and the analysis and design of uncoupled secondary components. Accordingly, the dynamic interaction between primary structures and process equipment is overlooked. The SPIF project – Seismic Performance of Multi-Component Systems in Special Risk Industrial Facilities – was carried out to respond to this gap, within the European H2020 SERA framework. Its objective regarded the investigation of the seismic behaviour of an archetype industrial multi-storey steel moment resisting frame (MRF) structure equipped with non-structural components (NSCs) by means of shaking table tests. The goal of the proposed study was to extend the interaction analysis between a primary multi-storey braced frame (BF) steel structure and NSCs in a performance-based earthquake engineering (PBEE) perspective. Along this vein, to excite the vibration periods of the NSCs and thus enhance possible coupling with the primary structure, a synthetic site-based ground motion model (GMM) was employed. More precisely, the proposed research intended: (i) to severely excite the process equipment and supplement the scarcity of real records with a specific frequency content by means of a stochastic GMM; (ii) to quantify seismic-induced force and displacement demands of secondary components and their effects on the primary BF structure. The evaluation of the experimental data clearly shows buckling in the bracing system of the BF configuration and a strong interaction between vertical tanks and floor crossbeams of the BF. At the very least, the favourable performance of the archetype BF under strong seismic records is demonstrated.

KEYWORDS
archetype steel braced frame, coupling interaction, ground motion model, industrial facilities, non-structural component, shake table testing

1 INTRODUCTION

1.1 Background and motivation

Past destructive earthquakes in China (Sichuan, 2008 and Yushu, 2010), Japan (Tohoku, 2011) and Italy (Emilia, 2012) have emphasized social and political attention on seismic risk arising from process plants. Both observations of damage following major/moderate seismic events[1] and numerical/experimental studies[2] have reaffirmed that petrochemical facilities are particularly and even disproportionately vulnerable to earthquakes. Besides, several researchers investigated numerous industrial accidents that have resulted in severe loss of life and injury, damage to natural and built environment as well as significant economic losses. As a matter of facts due to earthquake damage, it emerges that non-structural components (NSCs) and support systems interactions account for the majority of direct property losses.[3] In this respect, to collect and document the body of available knowledge related to the seismic performance of NSCs, the National Institute of Standards and Technology (NIST) invested on a year-long study summarized in Ref. [4]. From these studies, it clearly emerges: *(i)* a lack of definition of performance objectives for NSCs in a performance-based design methodologies perspective; *(ii)* a gap in performing fully comprehensive testing campaigns and investigations on coupling effects between primary structures and NSCs; *(iii)* a need to improve and enforce code requirements along with the development of reliable NSCs seismic demands models.

In recognition of *(i)*, that is, the absence of comprehensive non-structural performance objectives, NEHRP Provisions[5] proposed a framework for non-structural performance targets by delineating two categories of NSCs: *(a)* those not required to operate following a design basis earthquake (DBE); *(b)* and those expected to function following a DBE, defined in Ref. [6]. Despite their great importance, however seismic provisions for petrochemical facilities are based on classical load-and-resistance factor design (LRFD), like EN 1998-1,[7] VCI-Guideline,[8] or on allowable stress design (ASD), like ASME B31.1[9] and EN 13480[10]; a performance-based earthquake engineering (PBEE) approach should, instead, be preferred. Nevertheless, it is noteworthy that whilst several aspects in terms of design and analysis are still unresolved, code-compliant methods demonstrated to result in very poor predictions and often dated and inadequate, as highlighted in Refs. [11–13].

With regard to the *(ii)* issue, also Mosqueda et al.[14] underlined a definite lack of investigation as well as protocols for testing the interaction between primary structures and NSCs under seismic loading. As regards the analysis of global systems based on PBEE, only a few studies can be found.[14,15] For instance, the application of the PBEE to two realistic substructures of petrochemical piping systems showed a general overconservatism in piping system design. Conversely, some European research project, that is, INDUSE-2-SAFETY 2012–2015, clearly focused on experimental testing of NSCs and performance levels to be compliant with. To develop a better understanding of the elasto-plastic response and ultimate strength of nuclear power piping systems, other agencies carried out a multi-year test programme.[16] As a result, in view of the enhancement of structural integrity of industrial, energy and nuclear components, design guidelines and recommendations were issued.[6,17]

In this respect, also a recent European project was proposed: the SPIF project – *Seismic Performance of Multi-Component Systems in Special Risk Industrial Facilities*. More precisely, the objective of the SPIF project[18] was the investigation of the seismic behaviour of a representative industrial multi-storey frame structure equipped with complex process components by means of shaking table tests designed in a PBEE perspective. The testing campaign highlighted the dynamic interaction between the primary steel structure and secondary process units that clearly influenced the performance of the whole system.

On this latter aspect and strictly related to PBEE, the development of involved non-linear analysis methods for an accurate evaluation of both limit states and damage represents another salient issue.[19] Step-by-step dynamic integration of a structural system, where explicit nonlinear behaviour of both primary and secondary components is considered, is clearly the most reliable analysis method. Nonetheless, simplified approaches such as the non-linear static analysis or the use of floor response spectra (FRS) are generally preferred. Along the same vein, floor acceleration/displacement spectra represent a viable and promising approach which, however, have been applied to a lesser extent to the case of industrial structures, see Ref. [11]. For instance, Merino Vela et al.[11] focused on the development of floor acceleration spectra for an industrial concentrically braced frame (BF) supporting a liquid storage tank. The authors demonstrated that in most of the cases, code-compliant analytical approaches overpredict responses w.r.t. analyses that explicitly take into account the interaction between a supporting structure and a liquid storage tank. Moreover, recent studies, as in Refs. [12, 20, 21] investigated the main factors that mostly influence the amplification or decrease of FRS values:

inelasticity in the primary structure; location of the NSC in the supporting structure; periods of the component and main structure; involved damping ratio of the component. As results, improved equivalent-static equations were proposed for designing acceleration-sensitive NSCs, see Refs. [4, 20]. Besides, De Biasio et al.[12] selected intensity measures (IMs) capable of predicting NSCs acceleration demands and proposed a new IM, namely, the equipment relative average spectral acceleration ($E - ASA_R$). On this respect, to guarantee the IMs efficiency and sufficiency, a large and potentially expansible seismic dataset is required.

In addition to or in place of recorded motions, in recent years, there has been growing interest in earthquake ground motion models (GMMs) and in methods capable of generating synthetic ground motions, which can be used in PBEE. One method to generate synthetic motions relies on a site-based stochastic GMM, which directly describes the ground motion time-series recorded at a site. Recent examples of site-based stochastic GMMs include the non-stationary filtered white-noise model for far-field ground motions,[22,23] a wavelet-based model[24] and a multi-modal non-stationary spectral model.[25] All these models account for both temporal and spectral non-stationarity, which is an important characteristic of earthquake ground motions. Moreover, predictive relations for the model parameters were developed in terms of parameters describing the earthquake source and site characteristics. The predictive relations and stochastic model can then be used together to generate synthetic ground motions for any set of earthquake source and site characteristics of interest.

Inside this framework, the results of the SPIF project focused on an archetype MRF endowed with process equipment,[18,26] clearly showed how a proper experimental test campaign can highlight complex interactions between primary structures and NSCs. Besides, some left open issues aroused: *(i)* the test of the efficiency of other structural configurations as BFs; *(ii)* the selection of a seismic input capable of highlighting the coupling between primary structure and secondary elements. These are the issues that the paper explores further.

1.2 | Scope

Along this vein, the SPIF #2 project was conceived and realized by means of a shaking table test programme in a PBEE perspective. Thus, the present paper proposes limit states and performance objectives for a primary BF structure and NSCs; then, it presents the main results of the experimental campaign performed with a shaking table; successively, it compares experimental EDPs with reference values; and, eventually, it explains the interaction between the primary BF structure and the NSCs.

The paper comprises six sections; Section 2 provides a briefly overview of the SPIF project and its main findings. Then, Section 3 provides both limit states and performance objectives for a primary BF structure and NSCs; and deals with the design of the SPIF's mock-up for the BF configuration. Section 4 instead, presents the synthetic seismic signal employed and derived from a GMM selection and the shaking table test programme. More precisely, tests characterised by synthetic accelerogram levels ranging from 0.22*g* to 0.79*g* PGA, have been carried out. In Section 5, acquired data are assessed and system identification of modal frequencies, mode shapes and damping ratios is performed. Insights of the experimental data campaign are also provided with regard to seismic-induced force and displacement demands of secondary components, their effects on the primary structure and a comparison between experimental EDPs and reference values. Finally, main conclusions and outlooks are drawn in Section 6.

2 | THE PROJECT SPIF: LEARNED LESSONS FROM A MULTI-STOREY MOMENT RESISTING FRAME

The previous SPIF project,[18,26] focused on the investigation of the seismic behaviour of an archetype three-storey single-bay moment resisting frame (MRF) industrial substructure, tested by a uniaxial shaking table with several PGA's levels of a scaled spectrum-compatible record[7] described in Section 2.2. More precisely, the objective of the SPIF project was the investigation in depth of the dynamic interaction between the MRF steel structure and secondary process components – that influence the performance of the whole system in a performance-based perspective – as well as a proper check of floor spectra predictions. Both the case study considered with the relevant seismic input and the main results are presented herein.

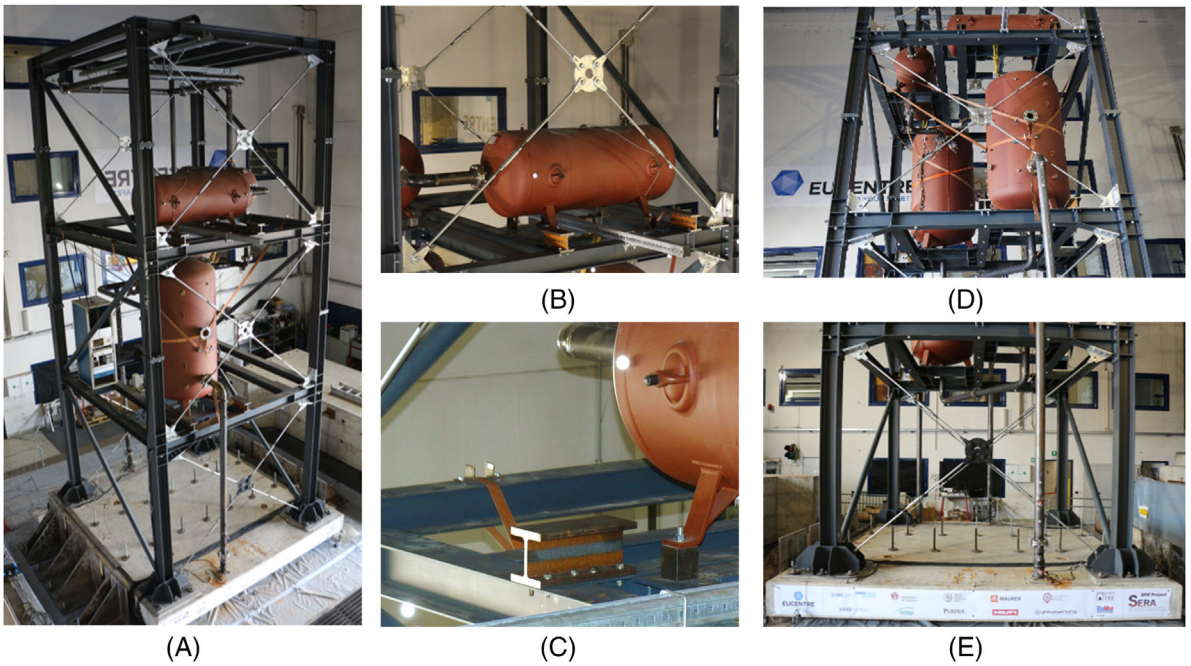

FIGURE 1 The SPIF #2 mock-up: (A) global view of the BF configuration; (B), (C) bracing system and T-stub connections of the intervention; (D), (E) front view of the 1st and 2nd floor at the EUCENTRE Laboratory

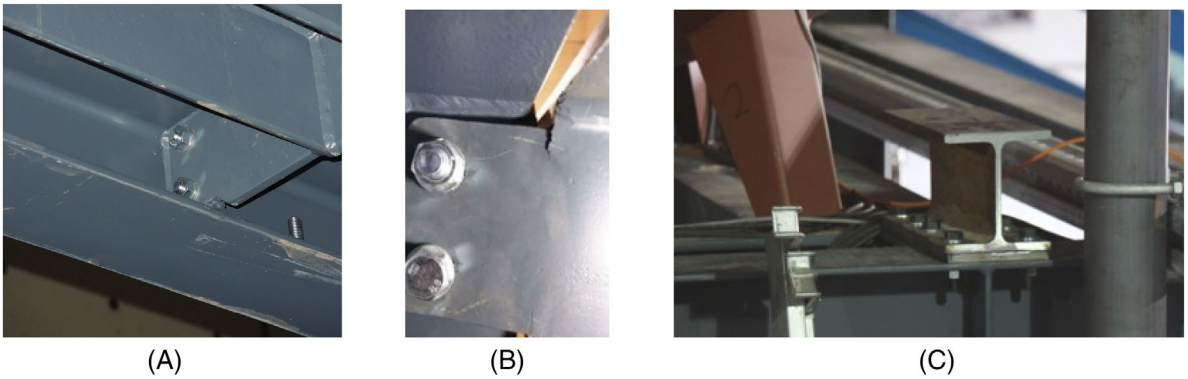

FIGURE 2 (A) Installed fin plate connections FP #1; (B) warping and crack propagation in the web of the crossbeam under Tank #2 and (C) strengthening intervention

2.1 | The case study

The original full scale mock-up consists of a primary steel structure supporting horizontal and vertical tanks, piping installations and a cabinet. Figure 1 gathers both photographs of the SPIF mock-up at the EUCENTRE Laboratory. Further information, construction details and greater insights on the SPIF campaign can be found in Refs. [18, 26].

Briefly, the mock-up was conceived as a three-storey steel grade *S*355 structure with flexible diaphragms made of crossbeams hinged to the frame beams. The dimensions of the designed structure are 3.7 m × 3.7 m in plan with a storey height of 3.1 m.

The horizontal load bearing system of the steel structure consisted of two MRFs in the direction of the seismic excitation and two BFs in the transverse direction equipped with tension/compression bracings with circular cross section. These latter were used in order to limit lateral movements and torsional effects. The two MRFs are connected through two BFs and crossbeams, which are fastened to the frame beams by simple bolted connections with web stiffeners; some photo of the beam-to-beam connection can be observed in Figure 2(A). These crossbeams served in turn as bearing supports for the installation of the NSC, that is, the secondary elements.

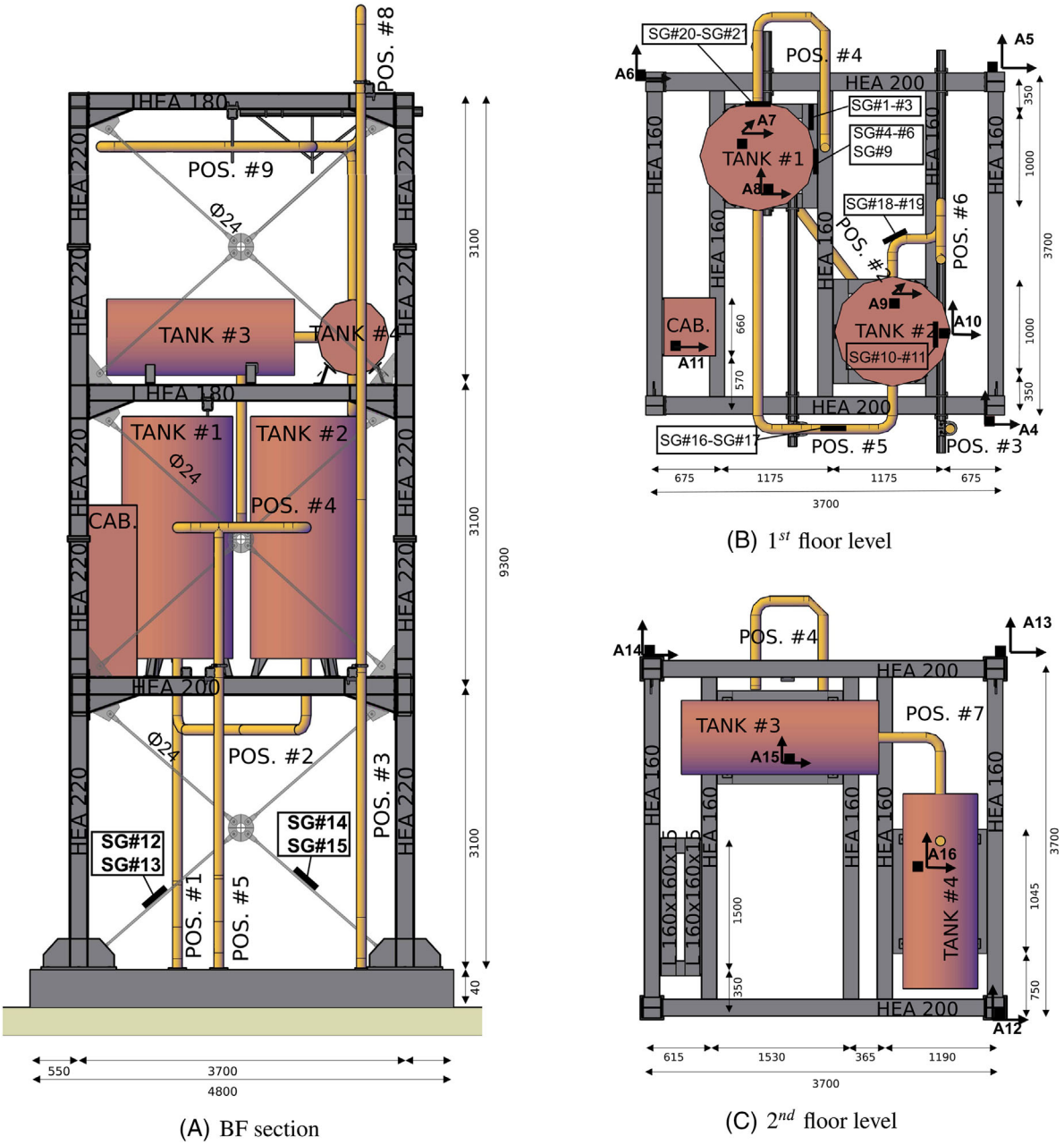

FIGURE 3 (A) Lateral view of the mock-up; (B) and (C) steel member layout, non-structural components and instrumentation

These secondary elements of the prototype industrial structure included tanks, pipes, elbows, bolted flange joints (BFJs), tee-pipe joints, a conveyor and a cabinet. More precisely, four unpressurized tanks made of steel $S235 - \texttt{JRG2}$ with a yield strength of 235 N/mm^2 were installed as indicated in Figure 3(B): *(i)* two vertical tanks on the first floor, that is, Tank #1 and #2; *(ii)* and two horizontal tanks on the second floor, that is, Tank #3 and #4, respectively. Their location reflects typical configurations in industrial installations. To simulate the liquid typically stored in such tanks, they were filled with granular material with a density equal to water. This allowed for the protection of the shaking table and technical installations against liquid release. The aforementioned tanks were mutually connected to each other through a piping system consisting of nine *DN*100 pipes, with a 100−mm diameter and a 3.6−mm thickness. Some pipes were also connected to the concrete slab. The relevant pipe layout consists of straight branches, elbows and tee pipe joints, as can be observed in Figure 1A–D. The material used for the pipes was *P*235 with a yield strength of 235 N/mm^2. In order to monitor the leakage detection, four branches of pipes (Pos.#1, #3, #4, #6) were filled with water and pressurized. Moreover, a suspended pipe rack was also installed on the third floor, endowed with *DN*80 pipes.

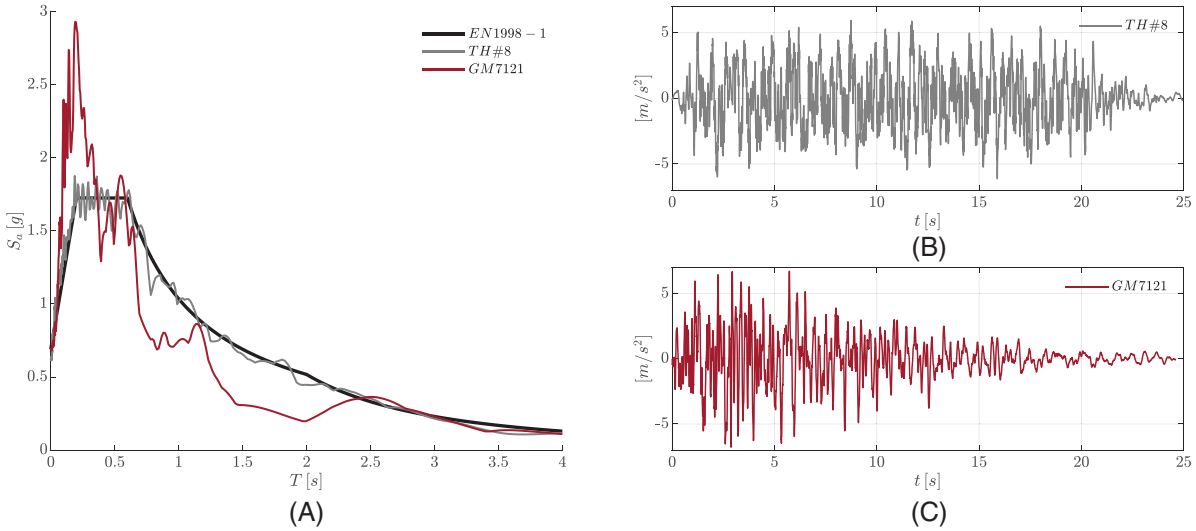

FIGURE 4 (A) Acceleration spectra according to: `EN 1998-1`, black line; `TH #8`, greyline, used in the SPIF MRF testing campaign; `GM7121`, red line, adopted in the SPIF #2 BF testing campaign. (B), (C) Relevant acceleration time histories of `TH #8` and `GM7121`, respectively

2.2 | Seismic inputs

Since the primary structure was designed to cope with the *Near Collapse* (NC) limit state, a severe earthquake prone-scenario was assumed leading to a design PGA of 0.69 g. Within a PBEE perspective, the mock-up was thus subjected to several shaking table tests, characterised by spectrum-compatible accelerogram levels ranging from 0.16 to 0.71-g PGA. In agreement with EN 1998-1,[7] these scaled accelerograms were based on a linear elastic response spectrum far field Type 1, with soil condition C, a PGA = 0.69 g and a damping ratio of 5%. The relevant spectrum is labelled as EN 1998-1 in Figure 4(A) with a black line. In addition, the seismic input assigned to the MRF configuration of the SPIF mock-up is named `TH #8` with a grey line in Ref. [26]. For the sake of completeness, the seismic input employed in the BF configuration of the SPIF #2 mock-up (red line) is labelled `GM7121`, and is described in depth in Section 4.1. Besides, time histories of acceleration of the assigned seismic input relevant to both the SPIF mock-up MRF and the SPIF #2 mock-up BF configuration are shown in Figure 4(B). In order to intensify potential coupling between the NSCs and the main structure, the `GM7121` signal was selected and adopted in the BF configuration of the SPIF #2 experimental campaign. A careful reader can notice that `GM7121` exhibits higher spectral intensities than the `TH #8` spectrum in the range period of the primary structure and NSCs, that is, between 0.05 and 0.25 s.

2.3 | Main results

Testing results definitely demonstrated a dynamic interaction between the primary MRF steel structure and secondary process units that clearly influenced the performance of the whole system. More precisely, the primary steel structure remained undamaged also for SSE earthquake levels mainly due to its design and inherent flexibility. In fact, the main steel structure characterized by a period of 0.36 s, enabled a filtering effect on the NSCs, whose periods, instead, ranged between 0.10 and 0.16. As a result, a strong interaction between the primary structure and the secondary components was avoided.

However, due to the use of common practice solutions for NSC components, inevitably some damage appeared in web plates of fin plate connections between main members and secondary beams. In fact, due to the strong rocking of the vertical tanks #1 and #2 during testing, the fin plate connection FP #1 shown in Figure 2(A), (B), clearly experienced warping of crossbeam's web and cracks in the transition zone from beam to web.

Moreover, in order to avoid further damage of the fin plate connection FP #1 and continue the test program at higher PGA levels, the crossbeam underneath Tank #2 was strengthened by means of a bolted T-stub depicted in Figure 2(C). As a result in the subsequent runs at higher PGA-levels, crack initiation, propagation and subsequent warping happened also in FP connections of other crossbeams underneath the vertical tanks.

3 | THE PROJECT SPIF #2: PERFORMANCE OF A MULTI-STOREY BRACED FRAME

3.1 | Rationale

Some open left issues of the previous SPIF test campaign aroused. More precisely: *(i)* the efficiency of other steel structure plant configurations; *(ii)* the deepening of the interaction between the primary structure and the NSCs. Therefore, to answer to these questions, the MRF was converted and tested with a BF configuration. As a result, a bracing system was conceived and designed as primary structure. As a result, we designed the bracing system following the EN 1998-1 [7] strength-based approach. Consequently, the natural frequencies of the heaviest tanks at the first floor, of about $f_{tank} = 6.25$ Hz and of the coupled braced structure became close. In addition, to emphasize the response of the coupled system at that frequency, we selected a proper seismic input with a significant frequency content in the range of interests of both the heavy tanks at the first floor and the BF. Due to damage of fin plate connections cited in Section 2.3, bolted T-stub connections were designed and added on secondary beams. For the sake of clarity, Figure 1 collects photos of the new configuration BF mock-up. More precisely, the overall view of the installed bracing system can be seen in Figure 1(A), whilst Figures 1(D) and 1(E) collect front views at the 1st and 2nd floor level. Besides, detail connections of the bracing system with the primary steel structure can be observed in Figure 1(B); while, in Figure 1(C), the strengthening intervention on secondary beams via bolted T-stub elements can be appreciated.

As regards the adopted bracing system, it is endowed with circular sections of 24-mm diameter and with a non-dimensional slenderness $\bar{\lambda} = 1.44$. As such, it was designed in compliance with the EN 1998-1[7] and the spectrum depicted in Figure 4(A), following the strength-based approach. For the sake of clarity, Figure 3(A) reports the BF configuration section, where both the bracing system and the NSCs can be clearly observed; while Figure 3(B), (C) depict the arrangement of the steel members and of the piping system layout of the first- and second-storey level, respectively. The seismic excitation `GM7121` depicted in Figure 4(C) was applied along the aforementioned direction. Moreover, both the sensing equipment and the relevant nomenclature of interests are depicted too.

As a result, the first period of the BF structure is equal to $T_1 \simeq 0.20$ s, which results to be significantly lower than that of the MRF $T_1 \simeq 0.35$ s. As anticipated, to enhance coupling effects between the primary structure and NSCs, the aforementioned ad hoc seismic input `GM7121` was selected. Therefore, severe floor acceleration spectra in the range periods of the equipment, that is, between 0.05 and 0.20 were induced. In particular, the heavy vertical tanks at the first floor, see Figure 3, whose periods approach 0.16 s have been excited.

3.2 | Performance-based design and reference limit states

According to the PBEE approach, the probability of exceeding specific damage states is quantified by using relevant thresholds, that is, limit states. Four common-practice limit states for civil engineering buildings are typically assumed and correlated to PGA levels: Fully Operational (FO), Damage Limitation, Significant Damage and NC, as defined in Ref. [27]. Multi-storey frame structures, like that of Figure 1, are typically considered as non-building structures for which the above-mentioned limit states are still considered applicable.[27] Conversely, performance objectives related to NSCs still remain an open issue. Along this vein,[28] defines the performance objectives for NSCs as FO, Position Retention (PR), Life Safety (LS) and Hazards Reduced (HR), which are related to increasing seismic intensity levels. With regard to NSCs installed in civil engineering structures,[28] prescribes that the FO limit state must be guaranteed for the lowest earthquake level whilst HR is the limit state associated to rare earthquakes. In this case, classical approaches classify NSCs as drift-sensitive and acceleration-sensitive, whose performance is based on global response parameters as inter-storey drift or absolute floor acceleration.[4] On the other hand, the same standard[28] prescribes that the FO limit state must be guaranteed for hazardous material storage also for higher earthquake intensity levels. Consequently, the limit states defined for civil structures have been reconsidered when applied to industrial plants.[2,15] Several standards, indeed, dealing with seismic analysis of chemical/petrochemical plants, for example,[27,29] among others, use the same limit states adopted by nuclear standards.[6] More precisely, they prescribe two distinct thresholds, namely the Design Basis (DBE) and the Safe Shutdown (SSE) earthquakes. DBE is defined as the condition under which facilities remain fully functional without undue risk to health and safety of people and is typically associated to a 10% probability of exceedance in 50 years, that is,

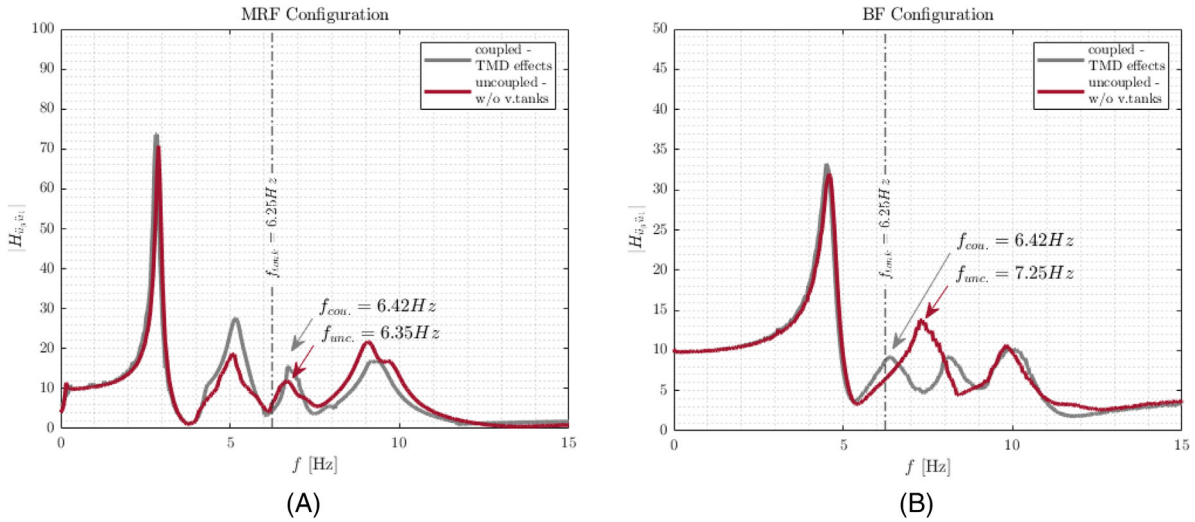

FIGURE 5 FRFs for the (A) MRF and (B) BF configurations: grey lines stand for numerical simulations results for the coupled system; red lines for numerical simulations without the two vertical tanks, installed at the 1st level

475 years,[29] and is modified using specific importance factors.[7] The SSE limit state is instead related to a lower probability of exceedance under which certain relevant structures, systems and important components must be designed to allow for a safe shutdown. The American standard[27] considers NSCs, that is, tanks, vessels, pipes and so forth as non-building structures for which dedicated standards are recommended.

Karamanos et al.[30] proposed performance criteria for liquid storage tanks and piping systems subjected to seismic loading that are useful for a quantitative definition of limit states for NSCs. In agreement with the above framework, both the definition of EDPs and thresholds adopted for primary structures and NSCs are summarized in Table 1. Thus, the seismic inputs correspond to DBE and SSE for both primary and NSCs and are linked to a probability of exceeding 10% and 5% in 50% in 50 years, respectively, with an importance factor of 1.5. In particular, for both storage tanks and pipes the thresholds are defined by strain thresholds, whilst the performance of the primary structure is governed in terms of inter-storey drift.[27] More precisely, the assumed minimum compressive strain ε_{Cu} for piping reads $\varepsilon_{Cu} = 0.5 \cdot (t/D) - 0.0025 + 3000 \cdot (\sigma_h/E)^2$; provided an internal pressure of 20 bar, see Section 2.1, it reaches a value of 1.6%.

3.3 | FE model of the primary steel structure

To comply with numerical, physical and control requirements of the experimental test campaign, a low fidelity (LF) FE model of the SPIF mock-up depicted in Figure 1 was deemed necessary. In particular, the LF model was initially adopted for the selection of the seismic input amplitude to be assigned to the shaking table; during the experimental campaign, then, the FE model was utilized to monitor and predict the response of the system, updated from run to run via SI. It was used in the post-processing phase, eventually, to better interpret the physical phenomena that governed the dynamic behaviour of the coupled system, for example, the TMD effects presented in Figure 5 and so forth. Thus, the SAP2000 software[31] was considered adequate for the complexity of the test-case structure. Linear elastic elements for the SPIF #2 structure have been generally adopted. Thus, columns and beams have been modelled by means of Euler–Bernoulli elements; floor levels diaphragms have been considered extreme flexible and, therefore, no-rigid constraints for each floor level were applied. In particular, in-plane and out-of-plane stiffness contribution was only provided by the grid location of secondary beams, as depicted in Figure 3(B), (C). Masses of cabinets and tanks were represented by lumped masses applied to ad hoc stick models, discussed in depth in the following Section 3.4 and reported in Figure 6(D), (E). A special attention was paid to the base joints. More precisely, to reproduce joint stiffness, a rotational link was adopted and calibrated against previously test run of the SPIF project; thus, an initial rotational stiffness $S_{j,ini} = 22.5$ MNm/rad was estimated through the FE Idea StatiCA®software.[32] Following 5.2.2.5(2) of EN 1993-1-8,[33] we have evaluated $S_{threshold} = 109.94$ MNm/rad, through

TABLE 1 Limit states and performance objectives for industrial plants

				Primary structure			NSC				
Limit states	P_{VR}	T_R	**PGA**	**Performance requirement**			**Performance requirement**	**Tank**		**Piping**	
DBE	10%	1200	0.56	All components devoted to normal operations remain functional. Damage to structure is limited. Structures do not experience permanent drift.	EDP	Performance threshold	Post-earthquake damage state in which the NSCs remain fully functional.	EDP	Performance threshold	EDP	Performance threshold
Design Basis					Storey drift	0.5%	Max tensile local strain	$\varepsilon<\varepsilon_y$	Tensile strain	$\varepsilon_t<\varepsilon_y$	
										Compressive strain	$\varepsilon_c<\varepsilon_y$
SSE	0.5%	2475	0.69	Minor yielding or buckling of braces. Transient drift that causes minor nonstructural damage. Negligible permanent drift.	Storey drift	1.5%	Post-earthquake damage state in which NSCs can be damaged, but they allow for a safe closure	Max tensile local strain	$\varepsilon_y<\varepsilon< 0.5\%$	Tensile strain	$\varepsilon_y<\varepsilon_t<0.5\%$
Safe Shut-down										Compressive strain	$\varepsilon_y<\varepsilon_c<\varepsilon_{C_u}$
											$\varepsilon_{Cu} = 0.5\cdot(t/D) - 0.0025 + 3000\cdot(\sigma_h/E)^2$

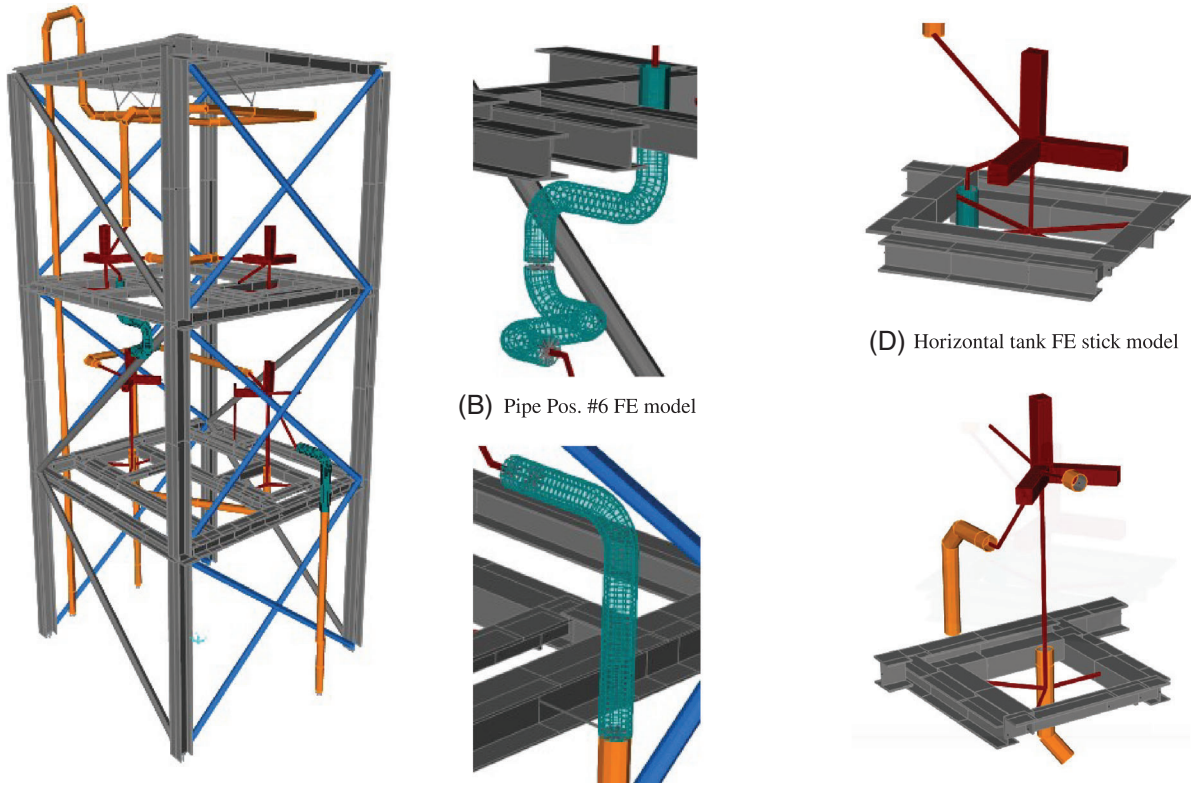

FIGURE 6 The SPIF #2 global FE model with relevant FE models of secondary components

Eq. (5.2d) that discriminates between rigid and semirigid joints. As $S_{j,ini}/S_{threshold} = 0.21$, we clearly deal with a semirigid joint. Moreover, the joint can be classified as a partial strength joint.

The Young's modulus was calibrated by means of previous tests and a value of 220 GPa has been assumed. Along this line, thanks to the rational fraction polynomials (RFPs) identification technique applied to the data collected from the previous experimental campaign, a damping ratio with a value of 4.5% was introduced as suggested by European[34] and nuclear standards. Non-linearities were introduced to model the bracing system through non-linear tension only elements. Figure 6(A) reports a sketch of the FE model of the BF configuration.

3.4 | FE models of the piping systems and secondary elements

To reduce the computational burden required by the analysis, the piping system and secondary elements, such as vertical and horizontal tanks, were the object of a thorough parametric analysis. Several techniques are available for modelling both the inherent flexibility and stiffness of piping system layouts, see for example,[30] that includes different components such as pipes, elbows, tee-joints and bolted flange joints (BFJs).

According to Ref. [10] tee-joints and straight pipes were modelled by means of beam elements with reduced stiffness' values through the adoption of flexibility factors. Instead, elbows, highly susceptible to ovalization and warping, were modelled with straight beam elements when it was possible to ensure a sufficient cut-off length. When this condition was not met, they were modelled with shell elements as depicted in Figure 6(B), (C) for piping system Position #1 and #6, respectively. Furthermore, BFJs were modelled by means of beam elements with springs at the ends calibrated against previous tests' data.[26] More precisely, following UNI EN1591-1,[35] the axial stiffness of 816 MN/m, the transversal stiffness of 313 MN/m and the rotational stiffness of 1.98 MNm/rad were estimated. For completeness, we have compared those stiffnesses to the ones of a 1-m length DN100 pipe, as in the monitored Pos.#1 configuration. Relevant ratios with regard to both rotational and shear stiffness entail that the BFJ is a semi-rigid joint; conversely, it is a pinned joint as far as the axial stiffness is concerned.

Moreover, tanks were modelled with simplified stick models, calibrated against previous outcomes of the SPIF campaign and validated through comparison of results from.[36] Following Ref. [34] both to consider the global seismic response and seismic action effects on the supporting structure due to the installed tanks, two modelling assumptions were made: (i) the particulate content moves together with the tank shell; (ii) the effective mass to consider is evaluated as 80% of the total mass of the granular content and is applied in correspondence of the tanks' centre of gravity. Therefore, in order to take into account both translational and rotational characteristics of the components, an equivalent stiffness for each considered degree of freedom has been evaluated and applied separately for each direction, as clearly depicted in Figure 6(D), (E) for both horizontal and vertical tanks.

At the very least, the predictive capabilities of the aforementioned LF model have been checked with results stemming from the experimental frequencies and mode shapes. In particular, to perform system identification (SI) in order to calibrate and validate the numerical model, we applied the RFP to the experimental frequency response functions (FRFs) provided by seismic inputs.

More specifically, we compute the matrix of FRFs obtained from seismic excitation signals of the shaking table and the corresponding response signals of the whole structure, processed at a sampling rate of 256 Hz. Then, to define the system's transfer function, we perform the ratios between outputs versus input in the frequency domain. In particular, we assume that the response to the input applied at location q is measured at location p, and thus, the related FRF reads

$$H_{pq}(\omega) = \frac{Y_p(\omega)}{F_q(\omega)} = \frac{\sum_{k=0}^{n} \beta_k (i\omega)^k}{\sum_{h=0}^{m} \alpha_h (i\omega)^k} \tag{1}$$

For a generic single input-multiple output case, Euation (1) can be expressed in a matrix form in the unknown α_h and β_k terms as

$$\sum_{h=0}^{m} \left([\alpha_h](i\omega)^k \right) \cdot [H(\omega)] = \sum_{k=0}^{n} \left([\beta_k](i\omega)^k \right) \tag{2}$$

Therefore, the unknown coefficients $(\alpha_h, h = 0, \dots, m)$ and $(\beta_k, k = 0, \dots, n)$ of both the numerator and denominator polynomials can be determined in a least-squared-error sense, by curve fitting the aforementioned analytical form to measurement data.

As demonstrated by Ref. [37] the denominator of the RFP holds the information about poles or eigenvalues of the structure, whilst the numerator embodies the information about the mode shapes or eigenvectors of the dynamic system. Consequently, frequencies, mode shapes and damping ratios of the BF structure were evaluated. Section 5.1 collects both results and insights of the SI procedure.

4 | INPUT SELECTION, SHAKE TABLE TEST PROGRAMME AND SENSOR LAYOUT

This section is particularly important because the performance of both the primary structure and NSC were established by means of several limit states. These states need to be clearly reached and exceeded by specific seismic excitation levels, and in this case, synthetic ground motions. Moreover, the shake table test program that incorporates different levels of input is presented and discussed.

4.1 | Input selection

In order to excite NSCs characterized by vibration periods of $T = 0.10 - 0.20$ s and possibly couple the secondary components to the primary BF structure, the accelerogram `TH #8` resulted to be inadequate due to its spectral properties shown in Figure 4(A). As a result, a synthetic GMM was employed also with purpose of reproducing the spectral variability of recorded accelerograms. Along these lines, the GMM proposed by Ref. [22] was assumed. The stochastic and site-located adopted GMM is based on a modulated and filtered white-noise process that incorporates both temporal and spectral

TABLE 2 Values of probabilities density distributions of GMM's parameters

Model parameters		Units	Distribution	μ	σ	Distribution bounds
I_a	Arias intensity	[m/s]	Log-normal	−0.46	0.51	$(0; +\infty)$
D_{5-95}	Time interval of 95% of the I_a	[s]	Log-normal	2.21	0.23	$(0; +\infty)$
t_{mid}	Time interval of 45% of the I_a	[s]	Log-normal	1.698	0.21	$(0; +\infty)$
$\omega_{mid}/2\pi$	Filter frequency at t_{mid}	[Hz]	Uniform	4.8	1	[3.8; 5.8]
ζ_f	Filter damping ratio	[-]	Uniform	0.35	0.1	[0.25; 0.45]

TABLE 3 Recorded natural seismic events selected as input for the GMM's dataset

Event name	Date	M_w [-]	Station	Epicen. Dist. [km]	PGA [g]	$V_{S.30}$ [m/s]
EMSC-20161030-0000029	30/10/2016	6.50	AMT	26.40	0.522	670
EMSC-20161030-0000029	30/10/2016	6.50	CSC	14.90	0.165	698
EMSC-20161030-0000029	30/10/2016	6.50	MSC	39.20	0.092	652
EMSC-20161030-0000029	30/10/2016	6.50	MZ08	26.40	0.527	670
EMSC-20161030-0000029	30/10/2016	6.50	MZ51	25.90	0.947	638
EMSC-20161030-0000029	30/10/2016	6.50	TERO	46.60	0.121	912
EMSC-20160824-0000006	24/08/2016	6.00	CSC	18.30	0.105	698
EMSC-20160824-0000006	24/08/2016	6.00	MSC	21.30	0.104	652
EMSC-20160824-0000006	24/08/2016	6.00	MTR	19.40	0.079	689
EMSC-20160824-0000006	24/08/2016	6.00	TERO	31.50	0.084	912
IT-2009-0121	09/04/2009	5.40	AQP	11.80	0.076	836
IT-2009-0102	07/04/2009	5.50	AQG	14.60	0.133	696
IT-2009-0102	07/04/2009	5.50	AQP	13.20	0.092	836
IT-1998-0103	09/09/1998	5.60	LRG	12.50	0.242	603
IT-1998-0103	09/09/1998	5.60	LRS	18.00	0.162	1024
IT-1980-0012	23/11/1980	6.90	BSC	28.30	0.094	972
IT-1980-0012	23/11/1980	6.90	CLT	18.90	0.171	557

non-stationarities, that is

$$a_g(t) = q(t, \widehat{\alpha}) \left[\frac{1}{\sigma_f(t)} \int_{-\infty}^{t} h(t - \tau, \lambda(\tau)) \omega(\tau) d\tau \right] \tag{3}$$

where $\omega(\tau)$ is a white-noise process and $\widehat{\alpha}$ is defined by means of

$$\widehat{\alpha} = arg \min_{\alpha} \left(|I_a(t_{45}) - \widehat{I}_a(t_{45})| + |(I_a t_{95}) - \widehat{I}_a(t_{95})| \right) \tag{4}$$

More precisely, $q(t, \widehat{\alpha})$ represents the modulating function that completely defines the temporal characteristics of the process. In addition, $h(t - \tau, \lambda(\tau)) = f(\omega_f, \zeta_f)$ is the impulse-response function (IRF) whose parameters thoroughly define the spectral characteristics of the process, with $\omega_f = \omega_{mid} + \dot{\omega}_{mid}(t - t_{mid})$ and ζ_f sets the filter damping ratio. With regard to Equation (4), $I_a()$ and $\widehat{I_a()}$, define the reference and the simulated Arias intensity evaluated at 45% and 95% of the Arias intensity, respectively; additional information can be argued from Table 2 and Ref. [22].

An initial dataset of recorded accelerograms was drawn both by the INGV catalogue[1] and ITACA – Italian Accelerometric Archive Database[2] – with the following requirements: (i) fault to site distance $R > 10$ km; (ii) moment magnitude $M_w > 5.5$; (iii) main shock seismic events only; (iv) strong motion intensities expressed in terms of $PGA > 0.075$ g.

Besides, to be consistent with the aforementioned `TH #8` spectrum-compatible accelerogram employed for the MRF mock-up, the soil condition $V_{S,30} > 600$ m/s and normal fault mechanism criteria were adopted. Table 3 gathers the set of

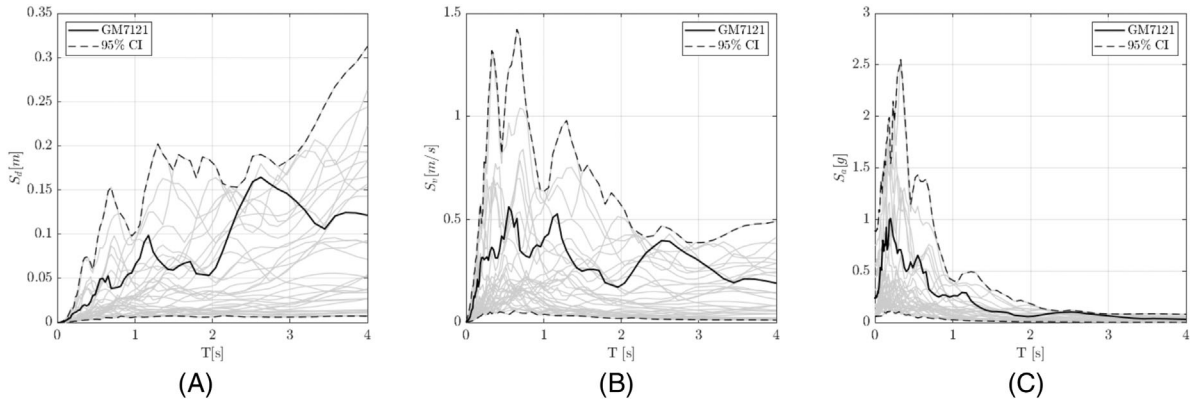

FIGURE 7 Selected records: (A) displacement; (B) velocity and (C) acceleration response spectra. Grey lines refer to single records whereas black dashed lines indicate the corresponding 95% confidence interval

selected natural seismic records, while Figure 7 highlights a good variability of the selected records in terms of frequency and intensity content for both the NS and WE components.

In agreement with the aforementioned requirements, a severe seismic prone zone of central Italy was identified and selected in Palmoli (CH), by means of a deaggregation probabilistic seismic hazard analysis (DPSHA). Owing to its low variability, a fixed value of frequency's change rate $\dot{\omega}_{mid} = -0.5\, rad/s^2$ was selected. Therefore, in order to calibrate the remaining five GMM parameters, that is, I_a, D_{5-95}, t_{mid}, ω_{mid} and ζ_f, against motion characteristics of the selected natural records, the relevant values of probability density distributions, which are gathered in Table 2 to the dataset collected in Table 3 were selected.

In order to set the number of white-baseline-noise processes, 100 values of $\omega(\tau)$ were combined to 100 parameter realizations according to the distributions defined in Table 2, so expanded to a total of 10, 000 synthetic accelerograms. It was observed that 100 values of $\omega(\tau)$ were enough to ensure a convergence of the 75th percentile of $S_a(T_1)$ for T_1 =0.18 and 0.36 s, respectively. Among the ensemble, the records were also checked w.r.t. shacking table limits, frequency content and spectral acceleration in the period's range of interest for the BF structure and its secondary components. Finally, the aforementioned `GM7121` record, depicted in Figure 4(C), was selected and adopted for the test campaign.

4.2 | Test programme

In the perspective of the PBEE approach discussed in Section 3.2 and defined in Table 1, the experimental campaign included different PGA levels for the test structure. Besides, in view of both the tuning of the shaking table and the dynamic identification of the mock-up, the test campaign was further enriched with a series of tests with random excitation and low PGA levels, between 0.05 and 0.15 g. Thus, the seismic excitation was then scaled w.r.t. the design PGA of 0.69g to 31%, 38%, 62%, 81%, 93%, 100% and 115%, respectively. The corresponding testing campaign and nomenclature is collected in Table 4. For instance, the first two runs were conducted with two random excitations, named RND #1 and RND #2. Successively, runs with PGA levels of 0.22, 0.26 and 0.43 g were carried out. Moreover, the most severe test was executed at the maximum value of 0.79-g PGA. Eventually, a closing test with the random excitation RND #9 was performed.

4.3 | Sensor layout

The sensor layout for the SPIF #2 test campaign remained basically unchanged from the first SPIF campaign. Therefore, for the sake of clarity, a careful reader is referred to Subsection 2.2 of Ref. [18]. Nonetheless, both the main sensors and the different locations of the new strain gauges (SG) are depicted in Figure 3 and commented herein. Since the sensitivity analysis carried out on the FE SPIF #2 model predicted no uplift mechanism in the column bases, the relative SGs sensors and those installed on the uplift bars were removed. Conversely, w.r.t. the entire piping system, the T-joint in pipe Pos. #5 is endowed with SGs#16-#17, the elbows in pipe Pos. #1 with SG#20–#21, and the BFJ in Pos. #6 with SG#22–#24 were accurately monitored. Moreover, three SGs sensors – SG#1 to #3 – were installed on the support beam under Tank #1. To

TABLE 4 Nomenclature. Characteristics and synthetic observations of the SPIF #2 Test Programme

Label	Excitation	Limit state	Scaling factor [%]	PGA level [g]	Observations
RND#1	Random	DBE-OP	–	0.08	– Overall elastic linear behaviour
RND#2	Random	DBE-OP	–	0.08	– Overall elastic linear behaviour
GM7121#31%	Seismic	DBE-OP	31	0.22	– Overall elastic linear behaviour
GM7121#38%	Seismic	DBE-DL	38	0.26	– Overall elastic linear behaviour
GM7121#62%	Seismic	DBE-DL	62	0.43	– Relevant rotation of the cross beam under the vertical Tanks #1-#2
					– Buckling of SE bracing system at 1st floor
RND#3	Random	DBE-OP	–	0.08	– Overall elastic linear behaviour
RND#4	Random	DBE-OP	–	0.14	– Overall elastic linear behaviour
GM7121#81%	Seismic	SSE-SD	81	0.56	– Buckling of bracing system at 1st floor
					– Severe stresses on bottom wall of Tank #1-#2
RND#5	Random	DBE-OP	–	0.14	– Overall elastic linear behaviour
GM7121#81%-2	Seismic	SSE-SD	81	0.56	– Severe stresses on bottom wall of Tank #1
					– Buckling of bracing system at 1st floor
RND#6	Random	DBE-OP	–	0.14	– Overall elastic linear behaviour
GM7121#93%	Seismic	SSE-SD	93	0.64	– Relevant rotation of the cross beam under the vertical Tanks #1-#2
					– Buckling of bracing system at 1st floor
					– SG #7 plasticization at bottom wall of Tank #2
RND#7	Random	DBE-OP	–	0.14	– Overall elastic linear behaviour
GM7121#100%	Seismic	SSE-NC	100	0.69	– Significative displacement of LVDT at Pipe POS #6
					– Buckling of bracing system at 1st floor
					– Relevant rotation of the cross beam under the vertical Tank #2
					and warping of the web of fin plate FP #1-#2
RND#8	Random	DBE-OP	–	0.14	– Overall elastic linear behaviour
GM7121#115%	Seismic	SSE-NC	115	0.79	– Cracking on previously detail FP #1 and #2 significantly increased
					– Yielding of LVDT at Pipe POS #6
					– Severe stresses on elbow Pipe POS #6
					– Buckling of bracing system at 1st floor
RND#9	Random	DBE-OP	–	0.14	– Overall elastic linear behaviour

check the stress levels on the tanks' wall, SGs #4–#5 and #10–#11 were installed on the bottom plate of both Tank #1 and Tank #2. To monitor also the stress level and to check for instability, four SGs were installed on the bracing system at the 1st floor as depicted in Figure 3.

5 | DATA ANALYSIS AND INSIGHT

Both the system identification (SI) of the SPIF #2 structure and relevant observations drawn from the experimental campaign are presented and discussed hereinafter. In particular, the huge amount of collected data provides insights both on the primary structure and NSCs performance. Besides, a special focus is given to the dynamic interaction between the primary structure and the secondary components, but also between the structure, the components and various representations of the seismic input.

5.1 | System ID of frequencies, mode shapes and damping ratios of the primary structure

To estimate the dynamic properties of the experimental mock-up, the RFP method, mentioned in Section 3.4, has been employed. The RFP technique overcomes many of the numerical analysis problems associated to parameter estimation

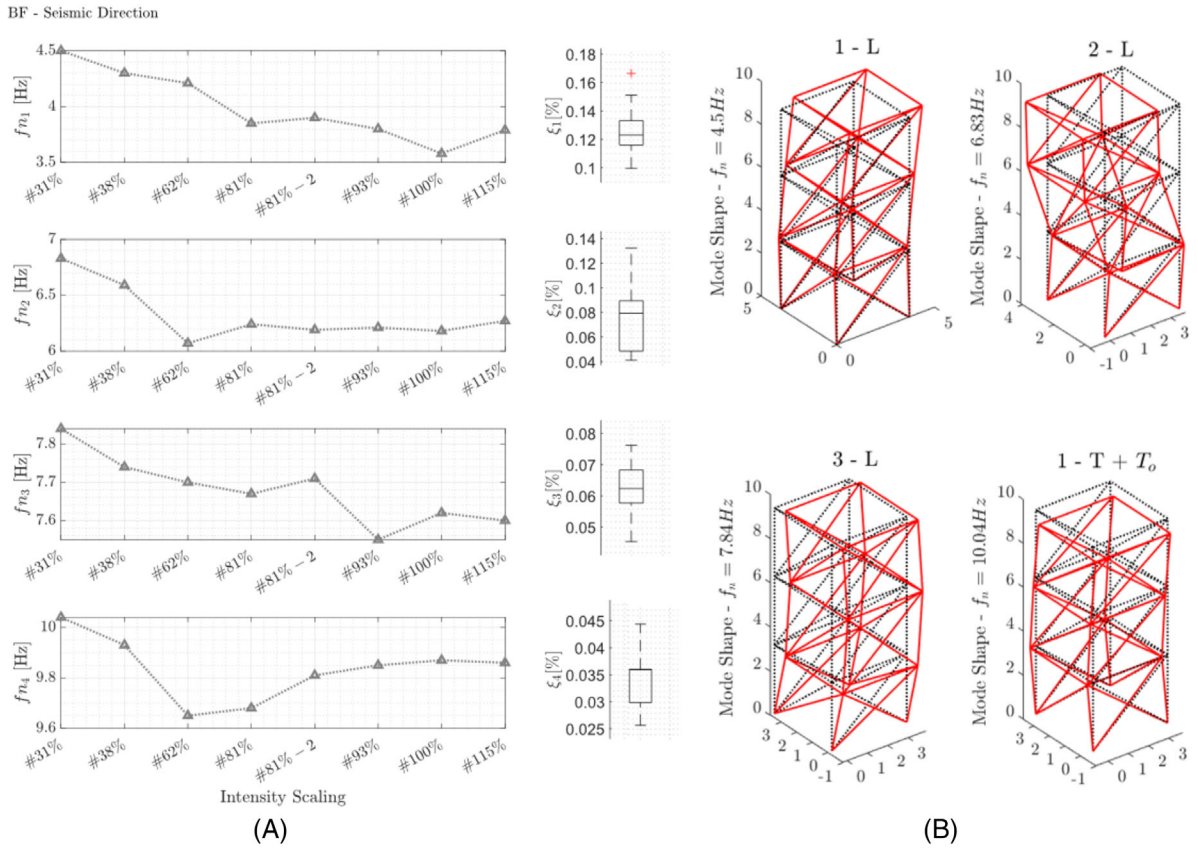

FIGURE 8 (A) Frequency variations for both the BF seismic direction relevant to the whole experimental programme. Damping ratio box-plots are reported with whiskers referring to the 10th and 90th-quantile; (B) mode shapes relevant to frequencies $f_n = 4.50, 6.83, 7.84$ and 10.04 Hz of Table 5

of structures, such as damping ratio estimation, processing computational burden and so forth; moreover, it allows for a quite accurate identification of poles, zeros and resonances. For the sake of brevity, Table 5 summarizes the main results in terms of eigenvalues – frequencies; while Figure 8(A), (B) collects frequencies, damping ratios and relevant mode shapes.

From Table 5, one can observe a slight decrease of frequency values in the DBE range, that is, until `GM7121#81%`. Conversely, a frequency jump from the DBE to the SSE range, that is, from 4.30 to 3.79 Hz for f_{n1}, can be clearly noticed. In addition, identified frequencies of the BF orthogonal system w.r.t. the BF seismic system have proven to be fairly consistent and indicate a limited amount of damage. Moreover, some frequencies in the BF orthogonal directions have not been identified due to the lack of power in the signals. Nonetheless, the reliability of the identified values is confirmed by the values of the coherence function.

Figure 8(A) depicts the natural frequencies of the identified modes, which clearly show a decrease after each seismic test; an exception is represented by the test run `GM7121#62%`, where the bracing system was subjected to elastic buckling with a subsequent stiffness recovery. The identified damping ratios reported in the same figure correspond to the first three modes of vibration, 1-L, 2-L and 3-L, and range between 5% and 16%. These high damping values are mainly due to the contribution of granular material stored in vertical Tanks #1 and #2, as stated also in Ref. [7]. On the other hand, the damping ratios of the modes associated with the deformation of the primary steel structure – modes 1-T+To – are mostly in the range 2.5%–4.5%.

Moreover, based on magnitude and phase of FRFs, the mode shapes of the tested structure have been derived and reported in Figure 8(B). They correspond to the first three longitudinal modes (1-L, 2-L, 3-L) and the first coupled transverse-torsional mode (1-T+To). The modes 1-L and 1-T-To mainly contribute to the deformation of the primary structure; while the modes 2-L and 3-L represent the dynamic response due to coupling interactions between NSCs, that is, the vertical Tanks #1 and #2, and the primary steel structure.

TABLE 5 Identified frequencies by means of the RFP's signal analysis on the `GMM7121` excitation for both the BF seismic and orthogonal direction. The horizontal line separates DBE from SSE seismic inputs. Also Δ[%] variations between current and initial frequencies are reported

BF – Seismic direction									**BF – Orthogonal direction**									
Input	$f_{n1}[Hz]$	**Δ**[%]	$f_{n2}[Hz]$	**Δ**[%]	$f_{n3}[Hz]$	**Δ**[%]	$f_{n4}[Hz]$	**Δ**[%]	**Input**	$f_{n1}[Hz]$	**Δ**[%]	$f_{n2}[Hz]$	**Δ**[%]	$f_{n3}[Hz]$	**Δ**[%]	$f_{n4}[Hz]$	**Δ**[%]
`GMM7121#31%`	4.30	–	6.83	–	7.84	–	10.04	–	`GMM7121#31%`	4.58	–	–	–	7.29	–	10.17	–
`GMM7121#38%`	4.50	−4.68	6.59	3.48	7.74	1.28	9.93	1.05	`GMM7121#38%`	4.08	10.9	–	–	7.85	−7.68	9.72	4.42
`GMM7121#62%`	3.65	15.08	6.07	11.07	7.70	1.70	9.28	7.51	`GMM7121#62%`	4.97	−8.51	6.24	–	–	–	9.42	7.37
`GMM7121#81%`	3.85	10.42	6.24	8.65	7.83	0.09	9.68	3.54	`GMM7121#81%`	4.83	−5.46	6.40	−2.56	–	–	9.64	5.21
`GMM7121#81%-2`	3.90	9.36	6.19	9.28	7.71	1.58	9.81	2.33	`GMM7121#81%-2`	4.31	5.89	6.37	−2.08	–	–	9.53	6.29
`GMM7121#93%`	3.80	11.65	6.21	8.98	7.55	3.64	9.85	1.83	`GMM7121#93%`	3.26	28.8	6.84	−9.62	–	–	9.79	3.73
`GMM7121#100%`	3.58	16.87	6.36	6.88	7.62	2.74	9.87	1.67	`GMM7121#100%`	4.35	5.02	6.56	−5.12	–	–	8.79	13.5
`GMM7121#115%`	3.79	11.94	6.27	8.23	7.78	0.72	9.92	1.14	`GMM7121#115%`	4.13	9.48	6.19	0.80	–	–	9.48	6.78

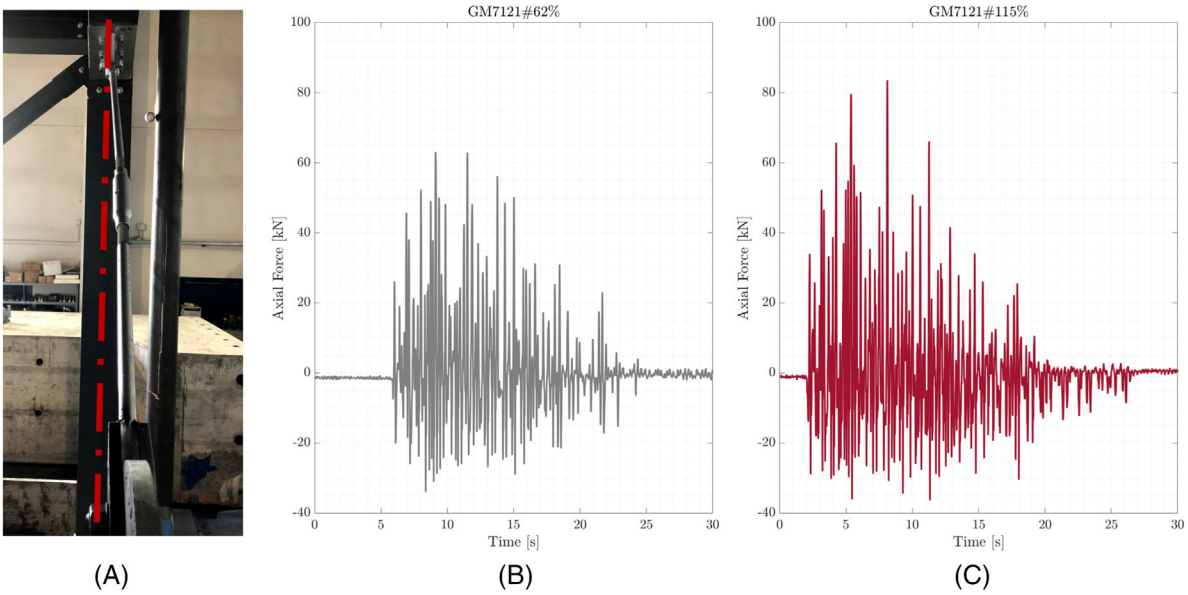

FIGURE 9 (A) Photo of a buckled brace at GM7121#62%; (B) axial forces time history at GM7121#62% and (C) at GM7121#115%

Both for brevity and a better comprehension of Section 5.4, the main frequencies of Tank#1 and Tank#2 were identified. They correspond to ∼ 6.2 and ∼ 7.1 Hz, respectively; these figures were largely influenced, indeed, by the kinematics of the granular content.

5.2 | Performance of the primary structure

The primary structure depicted in Figure 1 was subjected to the dynamic inputs collected in Table 4. A careful reader can argue from Table 4 that the main structure exhibited an elastic behaviour up to a PGA level of 0.43 g. Subsequently, secondary crossbeams experienced an inelastic behaviour followed by elastic buckling of the bracing system at the 1st floor. Later, significant web warping and cracking of the aforementioned FP#1–#2 connection happened, see Figure 2(B).

For clarity, Figure 9(A) depicts the deformed shape of a brace at the 1st level buckled at about 20 kN for the excitation GM7121#62%. The average axial forces revealed by SG#14-15, depicted in Figure 3(A), corresponding to the excitations GM7121#62% and GM7121#115% are shown in Figures 9(B) and 9(C), respectively. One can notice the asymmetric behaviour of braces due to elastic buckling at about 20 kN. The large values exhibited by braces in compression, for example, about 38 kN are mainly affected by the preloading of about 15 kN initially applied to braces. Despite the high acceleration values that exceeded the NC limit state PGA values and, the consequent damage suffered by braces, they exhibited a favourable behaviour as foreseen in the design phases.

5.3 | Behaviour of secondary components

Vertical tanks:

As anticipated in Section 4.3, both vertical and horizontal tanks were monitored. In particular, being vertical, we focused our attention on vertical Tank #1 – with sensor A#7 at the base and A#8 at the top of the tank, see Figure 3(B). As a result, the top acceleration increase appears quasi-linear with the PGA level; whilst the amplification of the base acceleration was almost constant for each run except for: (i) the run GM7121#62% where buckling of the bracing system occurred: (ii) the runs GM7121#100% and GM7121#115% where buckling broadened and localized non-linearities at the fin plate connections intensified. Both the effects of brace buckling and stress peak values beyond the yielding threshold of 388 and 245 MPa of tanks, respectively, indicate a localized plasticization of braces and tank base connections and justify the aforementioned behaviour. Moreover, a comparison of recorded acceleration data between sensors installed at floor level and at vertical tanks' bottom revealed some coupling effects, as described in depth in Section 5.4 by experimental processed

TABLE 6 Mass values and μ ratios

		Mock-up masses	
		MRF	**BF**
Frame	[ton]	≃ 19	≃19
2 Vert. tanks	[ton]	6	6
μ	–	0.32	0.32

TABLE 7 Modal masses and μ_{mod} ratios

		Modal values	
		MRF	**BF**
Modal frequency	[Hz]	6.42	6.83
$M_{coupled}$	[ton]	≃ 0.95	≃ 8.55
$M_{w/out\ v.Tanks}$	[ton]	≃ 0.59	≃2.34
μ_{mod}	–	0.51	0.82

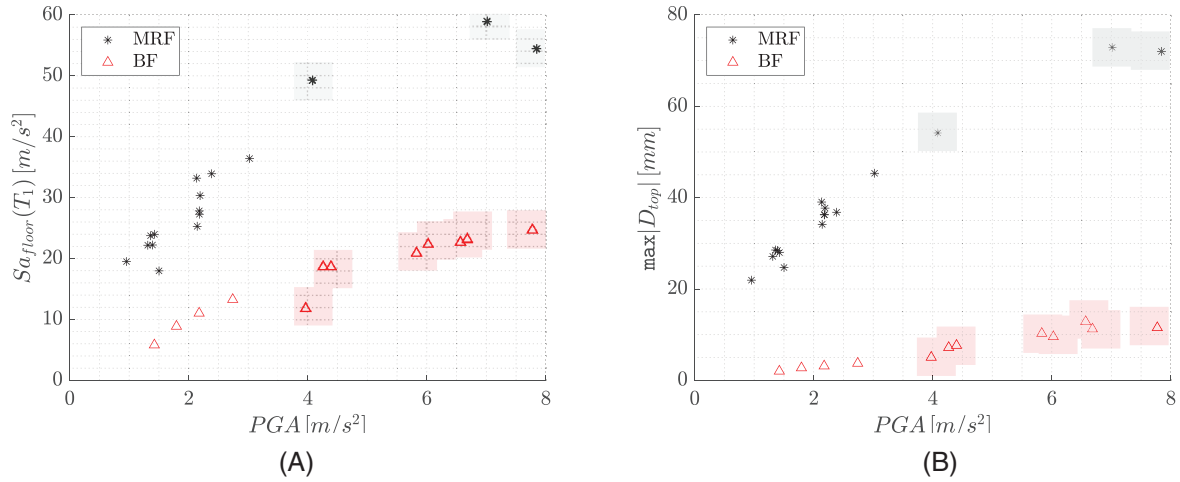

FIGURE 10 Seismic input versus primary structure correlation data: (A) PGA versus $Sa_{floor}(T_1)$ as spectral QoI; (B) PGA versus $\max|D_{top}|$ as non-spectral QoI. Collections of * and △ data represent results for MRF and BF configuration, respectively. Shaded dots indicate processed data after inelastic behaviour occurred

data. As noticed during the BF shaking table tests, the structural response was significantly reduced w.r.t. the previous MRF campaign, despite the adopted higher acceleration spectra input.

To better understand the above-mentioned phenomenon, Tables 6 and 7 together with Figure 5 have been prepared. Both table quantify the mass ratio $\mu = m_{Tanks}/m_{tot}$ and the modal mass ratio μ_{mod} of the heaviest tanks, that is, the vertical tanks located at the first floor, including Tank #1. Therefore, for brevity, the entailing coupling analysis is restricted at the first floor of MRF and BF configuration, respectively. Moreover, let' s consider Figure 5 that presents the FRFs for the MRF and BF configuration, respectively. In particular, grey lines stand for numerical simulations results related to the coupled system; red lines, instead, for numerical simulations without the 2 vertical tanks, installed at the first floor, whilst the vertical dash-dotted line indicates the natural frequency f_{tank} of the vertical Tank #1. One can clearly grasp two effects: *(i)* in Figure 5(B) related to the BF, the tuned mass damper (TMD) effect, that reduces the FRF amplitude at 7.25 Hz with the appearance of two lower adjacent peaks; *(ii)* the location of f_{tank}, which is in an antiresonance condition for the MRF configuration, see Figure 5(A), and in a resonance condition for the BF configuration, see Figure 5(B), with clear dynamic effects. One can look at De Angelis et al. [38] for additional considerations on TMDs with large masses. In such instances, the interplay between the primary structure, the vertical tanks and the seismic excitation can be better understood from Figures 10 to 11.

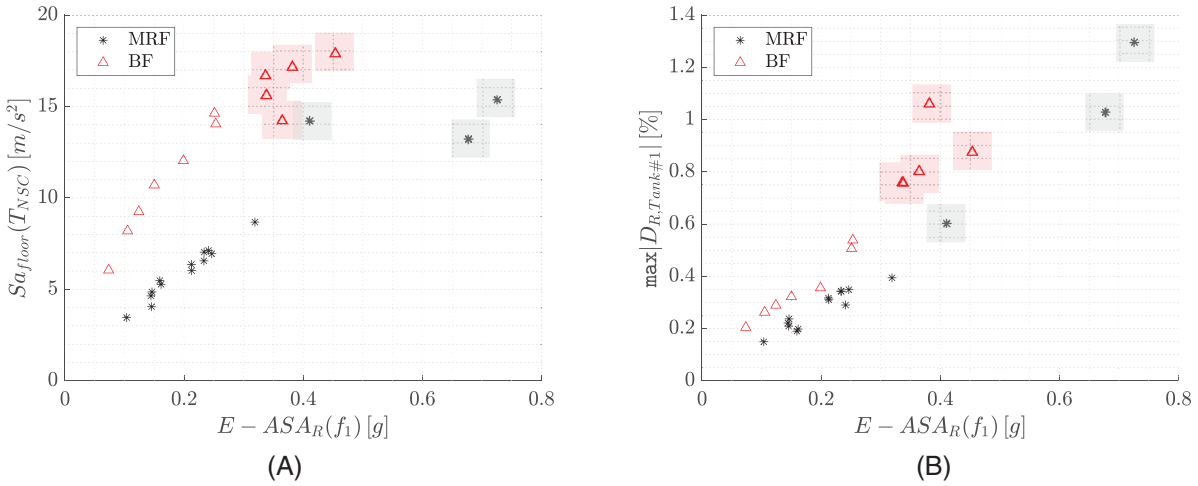

FIGURE 11 Primary structure versus NSCs correlation data: (A) $Sa_{floor}(T_1)$ versus $S_{V,Tank\#1}$; (B) $Sa_{floor}(T_1)$ versus $\max|D_{R,Tank\#1}|$. Collections of * and △ data represent results for MRF and BF configuration, respectively. Shaded dots indicate processed data after inelastic behaviour occurred

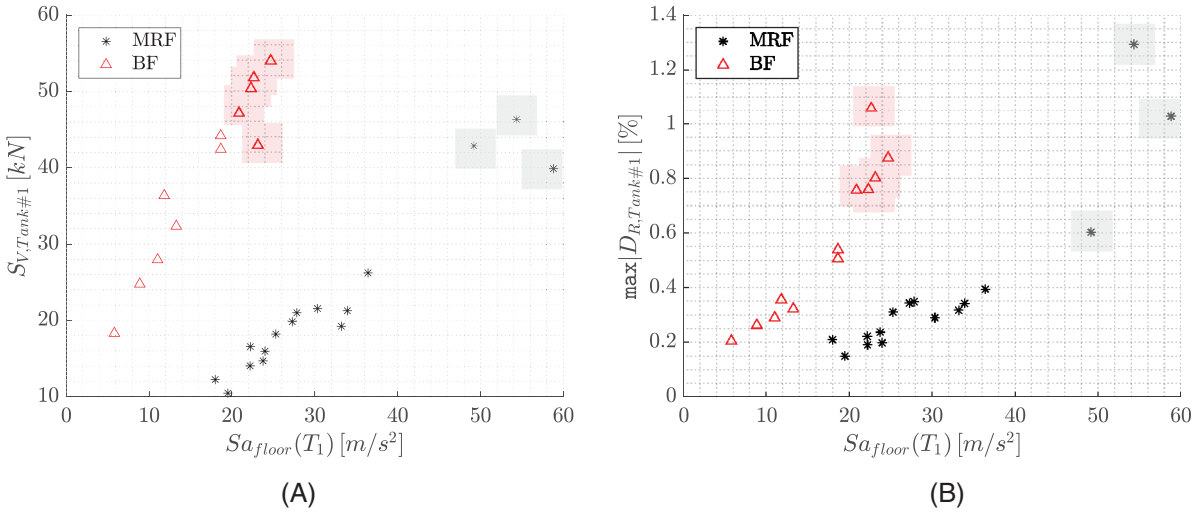

FIGURE 12 Pos.#1 BFJ: (A) sketch of the cross section; (B) photo of the monitored BFJ on site

Pipe connections: BFJs:

With regard to pipe connections, the BFJ category consists of a DN100-PN16 joint with loose flange and collar on one side and solid flanges on the opposite; M16x8 bolts and 2-mm aramid fibre gasket with NBR binder. For clarity, a schematic cross section of the water pressure (≃ 20 bar) Pos.#1 BFJ is depicted in Figure 12(A), whilst a photo of the monitored BFJ is reported in Figure 12(B). More precisely, to evaluate maximum values of flange opening and possible leakage, both SGs and LVDTs were installed. The leakage was also monitored with the use of optical fibres deployed in Pos.#4 BFJ, that is, one of the four pressurized pipe branches. A design tightening torque of 40 Nm was applied following the procedure described in Ref. [35]. In particular and in seismic condition, that tightening torque ensures a minimum gasket pressure $Q^L_{s,min}$ equal to 6 MPa that corresponds to a tightening class $L_{0,01}$.

In order to track leakage phenomena, previsions were made based on the analytical predictive model proposed in Ref. [39]. The model is based on the[35] framework; however, since it takes into account also the interaction with shear forces, it results to be more accurate and reliable than the standards.[35] This is confirmed in the experimental work documented in Ref. [40].

In detail, the analytical predictive model results in an interaction shear F_s – axial forces F_{RI} leakage domain as shown in Figure 13. It has been evaluated with an internal pressure of 20 bar and a friction coefficient $\mu = 0.15$. More precisely, F_{RI} defines the equivalent resultant axial force at the load condition stage I, evaluated as the joint contribution of the

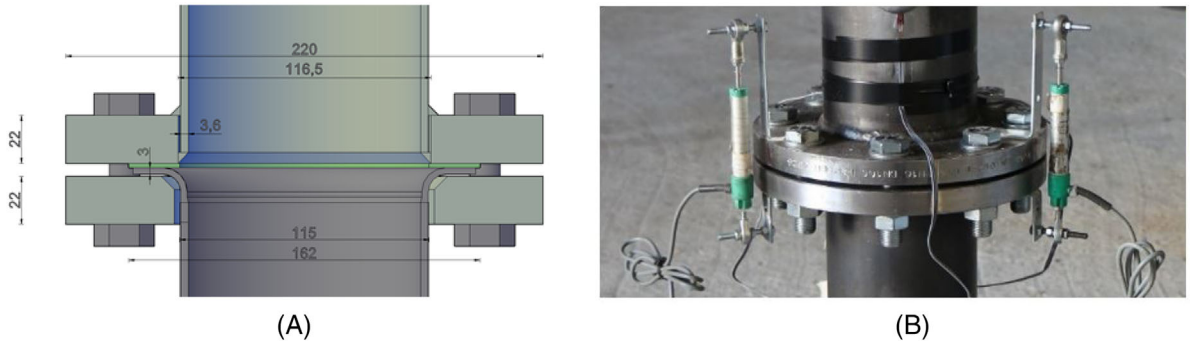

FIGURE 13 Leakage predictions and interaction domains with and w.o. safety factors for (A) DBE and (B) SSE condition

TABLE 8 Experimental EDP values and observed damage

		Primary structure			NSCs					
					Tank			Piping		
Limit state	PGA	Observed damage	EDP		Observed damage	EDP		Observed damage	EDP	
DBE	0.56	Minor buckling of the bracing system at the 1st floor	Storey drift	0.35%	Sever stresses on the bottom wall of Tank #1	Max tensile local strain	0.11%	–	Tensile strain	0.08%
									Compressive strain	0.07%
SSE	0.69	Buckling of the bracing system at the 1st floor. Warping in fin plate connections FP #1-#2	Storey drift	0.4%	Yielding on the bottom wall of Tank #1	Max tensile local strain	0.18%	Yielding of elbow in Pos. #6	Tensile strain	0.14%
									Compressive strain	0.12%

applied axial force and bending moment to the BFJ, that is

$$F_{RI} = F_{AI} + \frac{4}{\phi} \cdot M_{AI} \tag{5}$$

The resulting shear F_s – axial F_{RI} leakage domains for both the DBE and SSE scenario are depicted in Figures 13(A) and 13(B), respectively. More precisely, for each scenario, two interaction domains were set: (i) a domain that takes into account scatter effects due to the employed tightening technique method, according to Annex C and Annex F of Ref. [35] depicted by a continuous black line; (ii) a domain that does not take into account tightening scatter effects w.o. safety factors and depicted by a dashed black line.

In order to predict leakage of the entire set of BFJs, including the critical ones, that is, Pos.#1, #4 and #5 that were instrumented, the FE model described in Section 3.4 was employed. The aforementioned figures collect leakage predictions for all installed BFJs where the instrumented BFJs are highlighted in red. A careful reader can note that at DBE conditions, BFJs do not leak. Conversely, in the SSE scenario, leakage of BFJs is not expected, since all predictions are inside the leakage domain w.o. safety factors, as shown in Figure 13(B). These predictions were confirmed, indeed, both by visual inspection and data analysis provided by the test campaign.

In conclusion, Table 8 gathers EDPs values and observed damage, recorded during the experimental campaign, for the two limit states, thoroughly descripted in the previous Section 3.2. As a careful reader can notice, the recorded structural EDP values are far from the thresholds presented in Table 1. The reason for this is twofold: involved safety factors in the frame design; activation of large TMD effects, as mentioned in Section 5.3, that significantly reduced storey drifts. Instead, recorded EDPs and observed damage for NSCs are in good agreement with prescriptions of Table 1 of Section 3.2.

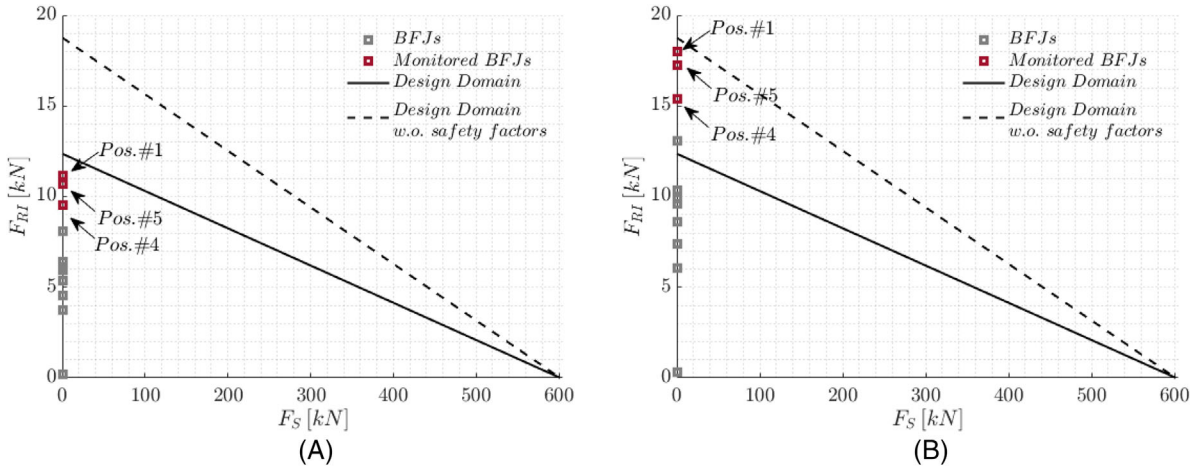

FIGURE 14 Seismic input versus NSCs correlation data: $E-ASA_R(f_1)$ versus (A) $Sa_{floor}(T_{NSC})$; (B) $E-ASA_R(f_1)$ versus $\max|D_{R,Tank\#1}|$. Collections of * and △ data represent results for MRF and BF configuration, respectively. Shaded dots indicate processed data after inelastic behaviour occurred

5.4 | Correlations between input, primary structure and non-structural components

The results of the comprehensive shake table test campaign on both the initial MRF and the BF configuration of the SPIF mock-up highlight the importance of understanding the correlation between: (i) the seismic input and the demand parameters of the structure; but also between (ii) the seismic input and the demand parameters of the NSCs; besides, when coupling effects are significant, informative directions and strengths of the relationships between (iii) seismic demand parameters of NSCs and the demand parameters of the primary structure can be found. To gain insights on potential correlations, several structural response quantities, NSCs demand parameters and seismic IMs were processed. Herein, main data findings are investigated for the two tested configurations, that is, MRF and BF, respectively, in terms of both spectral and non-spectral demand parameters.

Seismic input versus primary structure:
The investigated structural response quantities of interests (QoI) depicted in Figure 10(A), (B) are floor acceleration spectra evaluated at the fundamental period T_1 of the system and, maximum drifts recorded by markers at the last floor, respectively. In the X axis, we selected the PGA as informative IM of the input, among other quantities.[12] According to observations made during the experimental tests and summarized in Ref. [18] for the MRF and in Table 4 for the BF – where at a PGA level of 0.43-g brace buckling occurred, inelasticity was mainly observed in the steel structure; conversely, it was limited in the NSCs. As a result, the correlations observed are clearly non-linear. This is also evident looking at the forthcoming Figures 14 and 11.

In particular, see Figure 10(a), although the BF was more severely excited by the synthetic accelerogram of Figure 4, the structural response $Sa_{floor}(T_1)$ was more severe for the MRF, due to the favourable TMD effect exerted on the BF as explained in Section 5.3. Similarly, as expected, Figure 10(B) reveals the same trend, in terms of non-spectral maximum top displacements $\max|D_{top}|$; as a result, $\max|D_{top}|$ values of BF exceed those of the MRF.

Seismic input versus NSCs:
When NSCs are considered, see, in this respect, Figure 14 , it is deemed necessary to consider as QoI for the relevant demand parameters the maximum floor spectral acceleration $Sa_{floor}(T_{NSC})$ evaluated at the identified period $T_{NSC} \simeq 0.16$ s of the vertical tanks, and the maximum relative drift ratio of vertical tanks at the first floor, $\max|D_{R,Tank\#1}|$. This latter QoI is evaluated according to $D_{R,Tank\#1} = (\max D_{top,Tank\#1} - \max D_{base,Tank\#1})/H_{Tank\#1} \cdot 100$, where $\max D_{top/base,Tank\#1}$ stands for the maximum displacement recorded during each test, by the installed markers at the top and at the base level of Tank#1. With regard to the seismic input, along the indications of De Biasio et al.,[12] we adopt the innovative equipment relative average spectral acceleration, namely $E-ASA_R(f_1)$. More precisely, $E-ASA_R(f_1)$ is defined as the

average spectral pseudo-acceleration over the dominant-frequencies interval of the primary structure,

$$E - ASA_R(f_1) = \frac{1}{f_1 (X_f - 1)} \int_{f_1}^{X_f \dot{f}_1} S_a(f, \xi)\, \mathrm{d}f \tag{6}$$

where X_f is a factor accounting for the drop of the fundamental frequency f_1 of the primary structure, S_a is the spectral pseudo-acceleration and ξ defines the structural damping ratio. The suffix R indicates the chosen percentage of drop of the fundamental frequency ($X_f = 1 - (R/100)$). Anew, as the location of f_{tank} is in an antiresonance condition for the MRF configuration, see Figure 5(A) and in a resonance condition for the BF configuration, Figure 14(A) highlights the greater response in terms of $Sa_{floor}(T_{NSC})$ for the BF configuration.

Along the same line, $\max|D_{R,Tank\#1}|$ values of BF exceed those of the MRF.

Primary structure versus NSCs:

Anew, we deal with NSCs and primary structure characteristics. Therefore, a meaningful QoI of interest for the primary structure is $Sa_{floor}(T_1)$. We assume instead as QoI for the NSCs both the spectral shear base $S_{V,Tank\#1}$ and the non-spectral maximum relative drift ratio $\max|D_{R,Tank\#1}|$ of Tank #1. In particular, $S_{V,Tank\#1}$ is evaluated as $S_{V,Tank\#1} = m_{Tank\#1} \cdot Sa_{floor}(T_{Tank\#1})$, with a clear meaning of the terms. As $S_{V,Tank\#1}$ is proportional to $Sa_{floor}(T_{NSC})$, the same trend observed in Figure 14(A) is expected. As a consequence, also the maximum $|D_{R,Tank\#1}|$ is generally more intense for the BF configuration at equal spectral acceleration levels.

6 | CONCLUSIONS AND OUTLOOKS

The SPIF project, developed inside the European H2020 SPIF research framework, focused on the investigation of the seismic behaviour of an archetype multi-storey MRF structure equipped with complex secondary industrial components by means of shaking table tests. The experimental campaign was comprehensive and successfully carried out at the EUCENTRE Laboratory of Pavia and the tests clearly pointed out the inadequacy of floor crossbeams and routine design of fin plate connections. The existing SPIF MRF mock-up was converted into a BF configuration, by installing a dedicated bracing system. The mock-up was tested by means of a shaking table with several earthquake levels within a PBEE perspective. Thus, the present paper proposed limit states and performance objectives for a primary BF structure and NSCs; and to excite the vibration periods of the NSCs, that is, the heaviest vertical tanks, a synthetic record derived by a site-based GMM was selected; as a result, the complex interaction between the primary BF structure and the NSCs was enhanced; and the experimental EDPs values were compared with reference thresholds.

As a result, the SPIF#2 testing program was able (i) to highlight the efficiency of the BF configuration; (ii) to experimentally verify the effectiveness of the proposed PBEE limit states and thresholds; (iii) to provide data about the dynamic interaction between the primary steel BF and the NSCs; (iv) at the very least, to interpret the causes of these interactions. More precisely, the primary steel structure designed at the NC limit state exhibited almost a linear behaviour until the foreseen buckling of the bracing system at the first level. With regard to the NSCs performance, leakage phenomena at the monitored bolted flange joints did not occur, as predicted by analytical formulations based on design codes. Conversely, due to the behaviour of the heavy vertical tanks on secondary beams, the strong dynamic interaction between primary structure and NSCs was evident. In this respect, experimental relationships between several structural QoI, NSCs response parameters and PGA were determined. They showed that: (i) vertical tanks at the first floor acted as TMDs for the BF, and thus, the relevant base shear at the first floor was limited; this trend was also confirmed by frequency response functions; (ii) owing to dynamic properties, the favourable TMD effect was not relevant for the MRF configuration; (iii) owing to the flexible behavior of the secondary beams, vertical tanks induced warping of the web and crack propagations in the same beams and fin plate connections. In summary, a proper experimental test campaign on an archetype braced steel frame showed: (i) the effectiveness of a proper installed bracing system; (ii) the high influence of NSCs on the primary structure due to dynamic interaction. To enhance understanding of these complex systems and to improve current standards, low and high fidelity models calibrated on experimental data are needed for reliability evaluations.

ACKNOWLEDGEMENTS

The research leading to these results has received funding from the European Community's HORIZON 2020 Framework Programme [H2020-INFRAIA-2016-2017/H2020-INFRAIA-2016-1] for access to EUCENTRE Laboratory under grant agreement n^o 730900 – SERA project and from the Italian Ministry of Education, University and Research (MIUR) in the frame of the *Departments of Excellence* (Grant L232/2016).

Open Access Funding provided by Universita degli Studi di Trento within the CRUI-CARE Agreement.

DATA AVAILABILITY STATEMENT

The data that support the findings of this study are available from the corresponding author upon reasonable request.

ORCID

Chiara Nardin https://orcid.org/0000-0001-5860-0314
Oreste S. Bursi https://orcid.org/0000-0003-3072-7414
Fabrizio Paolacci https://orcid.org/0000-0003-2724-4809
Alberto Pavese https://orcid.org/0000-0003-4616-7693

ENDNOTES

[1]Istituto Nazionale di Geofisica e Vulcanologia, http://terremoti.ingv.it/en, accessed: 2020-08-01.
[2]ITalian ACcelerometric Archive v3.1, http://itaca.mi.ingv.it/, accessed: 2020-08-01.

REFERENCES

1. Brunesi E, Nascimbene R, Pagani M, Beilic D. Seismic performance of storage steel tanks during the May 2012 Emilia, Italy, earthquakes. *J Perform Constr Facil*. 2015. https://doi.org/10.1061/(ASCE)CF.1943-5509
2. Bursi O, Reza MS, Abbiati G, Paolacci F. Performance-based earthquake evaluation of a full-scale petrochemical piping system. *J Loss Prev Process Ind*. 2005;33. https://doi.org/10.1016/j.jlp.2014.11.004
3. Filiatrault A, Christopoulos C, Stearns C. *Guidelines, Specifications and Seismic Performance Characterization of Nonstructural Building Components and Equipment* [PEER Report 2002/05]. Berkeley, CA: University of California; 2001.
4. NIST GCR 18-917-43. *Recommendations for Improved Seismic Performance of Non-Structural Components*. 2018.
5. NEHRP. *Recommended Seismic Provisions for New Buildings and Other Structures*. 2015.
6. ASCE/SEI. Seismic Analysis of Safety-Related Nuclear Structures. *Standard 4-16*. ASCE/SEI; 2016.
7. European Committee for Standardization. *Design of Structures For Earthquake Resistance Eurocode* [4-16]. 2004.
8. *VCI-Guideline: Guideline, Seismic Design in Process Industry*. German Chemical Industry Association; 2013.
9. American Society of Mechanical Engineers. *Power Piping*. Washington DC: ASME B31.1 Standard; 2012.
10. European Committee for Standardization. *Metallic Industrial Piping - Part 3: Design and Calculation* [EN 13480-3]. 2011.
11. Merino Vela RJ, Brunesi E, Nascimbene R. Derivation of floor acceleration spectra for an industrial liquid tank supporting structure with braced frame systems. *Eng Struct*. 2018;171:105–122.
12. De Biasio M, Grange S, Dufour F, Allain F, Petre-Lazar I. Intensity measures for probabilistic assessment of non-structural components acceleration demand. *Earthq Eng Struct Dyn*. 2015. https://doi.org/10.1002/eqe.2582
13. Calvi P, Sullivan TJ, Nascimbene R. Towards improved floor spectra estimates for seismic design. *Earthq Struct*. 2013;4:109–132.
14. Mosqueda G, Retamales R, Filiatrault A, Reinhorn A. Testing facility for experimental evaluation of non-structural components under full-scale floor motions. *Struct Design Tall Special Build*. 2009. https://doi.org/10.1002/tal.441
15. Bursi O, Paolacci F, Reza MS, Alessandri S, Tondini N. Seismic assessment of petrochemical piping systems using a performance-based approach. *J Pressure Vessel Technol*. 2016;138:06. https://doi.org/10.1115/1.4032111
16. U.S.NRC. Seismic Analysis of Large-scale Piping Systems for the JNES-NUPEC Ultimate Strength Piping Test Program. Office of Nuclear Regulatory Research; 2008.
17. U.S. Department of Energy. Seismic Evaluation Procedure for Equipment in U.S. Deparment of Energy Facilities. Office of Defense Programs and Office of Environment, Safety and Health; 1997.
18. Butenweg C, Bursi OS, Paolacci F, et al. Seismic performance of an industrial multi-storey frame structure with process equipment subjected to shake table testing. *Eng Struct*. 2021. https://doi.org/10.1016/j.engstruct.2021.112681
19. Wang Z, Pedroni N, Zentner I, Zio E. Seismic fragility analysis with artificial neural networks: application to nuclear power plant equipment. *Eng Struct*. 2018. https://doi.org/10.1016/j.engstruct.2018.02.024
20. Sankaranarayanan R, Medina R. Acceleration response modification factors for nonstructural components attached to inelastic moment-resisting frame structures. *Earthq Eng Struct Dyn*. 2007. https://doi.org/10.1002/eqe.724
21. Anajafi H, Medina RA. Evaluation of ASCE 7 eqs. for designing acceleration-sensitive nonstructural components using data from instrumented buildings. *Earthq Eng Struct Dyn*. 2018. https://doi.org/10.1002/eqe.3006
22. Rezaeian S, Der Kiureghian A. Simulation of synthetic ground motions for specified earthquake and site characteristics. *Earthq Eng Struct Dyn*. 2010. https://doi.org/10.1002/eqe.997

23. Dabaghi M, Der Kiureghian A. Stochastic model for simulation of near-fault ground motions. *Earthq Eng Struct Dyn*. 2017;46(6):963-984. https://doi.org/10.1002/eqe.2839
24. Yamamoto Y, Baker J. Stochastic Model For Earthquake Ground Motion Using Wavelet Packets. 2011;103. https://doi.org/10.1201/b11332-366
25. Vlachos C, Papakonstantinou K, Deodatis G. A multi-modal analytical non-stationary spectral model for characterization and stochastic simulation of earthquake ground motions. *Soil Dyn Earthq Eng*. 2016. https://doi.org/10.1016/j.soildyn.2015.10.006
26. Butenweg C, Lanese I, Rizzo Parisi E, et al. Seismic Performance of Multi-component Systems in Special Risk Industrial Facilities. [Technical report, Deliverable D10.1, SERA Project, Project. No: 730900, H2020-EU 2020].
27. ASCE/SEI. Minimum Design Loads and Associated Criteria for Buildings and Other Structures. *Standard 7-16*; 2016.
28. ASCE/SEI. Seismic Evaluation and Retrofit of Existing Buildings. *Standard 41-17*; 2017.
29. Association ENFP. Standards for the Production. *Storage and Handling of Liquefied Natural Gas (LNG)*; 2006.
30. Vathi M, Karamanos S, Kapogiannis I, Spiliopoulos K. Performance criteria for liquid storage tanks and piping systems subjected to seismic loading. *J Pressure Vessel Technol*. 2017;05:139. https://doi.org/10.1115/1.4036916
31. Computers and Structures, Inc. *SAP2000 Version 21.1.0 Ultimate*. Berkeley, CA: Computers and Structures, Inc; 2019.
32. Idea StatiCA®2009-2022. *Idea StatiCA – Steel Connections*. 2021.
33. European Committee for Standardization. *Eurocode 3 – Design of steel Structures Part 1–8: Design of Joints* [CEN/TC 250]. Brussels; 2005.
34. European Committee for Standardization. *Eurocode 8 – Part 4: Silos, Tanks and Pipelines*. 2004.
35. UNI EN 1591-1. *Design Rules for a Gasketed Circular Flange Connection – Part 1: Calculation Method*. 2014.
36. Pieraccini L, Palermo M, Silvestri S, Gasparini G, Trombetti T. *Seismic horizontal forces exerted by granular material on flat bottom silos: experimental and analytical results*. 2016. Challenges in Design and Construction of an Innovative and Sustainable Built Environment. https://doi.org/10.2749/stockholm.2016.1050
37. Rainieri C, Fabbrocino G. *Operational Modal Analysis of Civil Engineering Structures – An Introduction and Guide for Applications*. Springer; 2014.
38. De Angelis M, Perno S, Reggio A. Dynamic response and optimal design of structure with large mass ratio TMD. *Earthq Eng Struct Dyn*. 2012;41:41–60. https://doi.org/10.1002/eqe.1117
39. Bursi O, di Filippo R, La Salandra V, Pedot M, Reza MS. Probabilistic seismic analysis of an LNG subplant. *J Loss Prev Process Ind*. 2017;10:53. https://doi.org/10.1016/j.jlp.2017.10.009
40. Paolacci F, Quinci G, Nardin C, Vezzari V, Marino A, Ciucci M. Bolted flange joints equipped with FBG sensors in industrial piping systems subjected to seismic loads. *J Loss Prev Process Ind*. 2021. https://doi.org/10.1016/j.jlp.2021.104576

How to cite this article: Nardin C., Bursi OS, Paolacci F, Pavese A, Quinci G Experimental performance of a multi-storey braced frame structure with non-structural industrial components subjected to synthetic ground motions. *Earthquake Engng Struct Dyn*. 2022;1–24. https://doi.org/10.1002/eqe.3656